Electronic Supplementary Material (ESI) for Journal of Materials Chemistry A.

Electronic Supplementary Information:

Achieving Excellent Activity and Stability for Oxygen Reduction Electrocatalysis by Hollow Mesoporous Iron-Nitrogen-Doped Graphitic Carbon Spheres

Tingsheng Zhou,[ab] Yao Zhou,[a] Ruguang Ma,[a] Qian Liu,[ac*] Yufang Zhu,[b*] and Jiacheng Wang[ac*]

[a] State Key Laboratory of High Performance Ceramics and Superfine Microstructure, Shanghai Institute of Ceramics, Chinese Academy of Sciences, 1295 Dingxi Road, Shanghai 200050, P. R. China.

[b] School of Materials Science and Engineering, University of Shanghai for Science and Technology, 516 Jungong Road, Shanghai 200093, P. R. China.

[c] Shanghai Institute of Materials Genome, Shanghai, P. R. China.

*Email - Jiacheng.wang@mail.sic.ac.cn

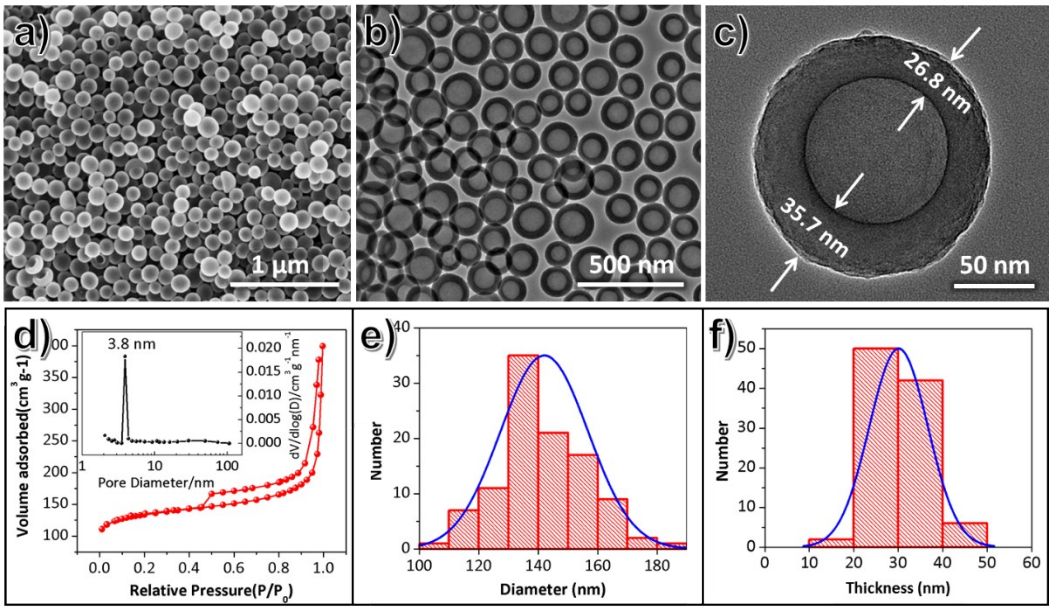

Fig. S1 a) SEM image, b-c) TEM images, d) Nitrogen adsorption-desorption isotherms and pore size distribution (inset), e) particle size distribution, and f) shell thicknesses distribution of the hollow polymer spheres (HPS).

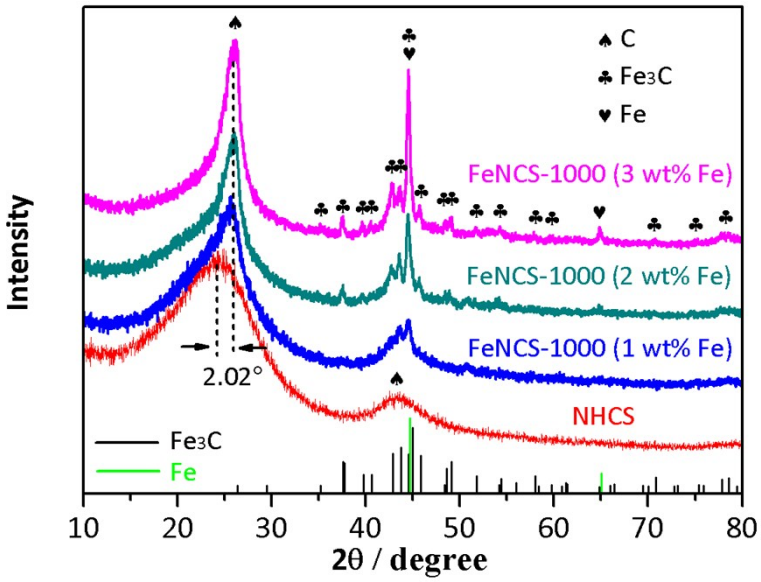

Fig. S2 XRD patterns of NHCS and FeNCS-1000 with 1, 2 and 3 wt% Fe. The diffraction peaks

ascribed to Fe/Fe_3C evidently increase with increasing the Fe content in the precursors.

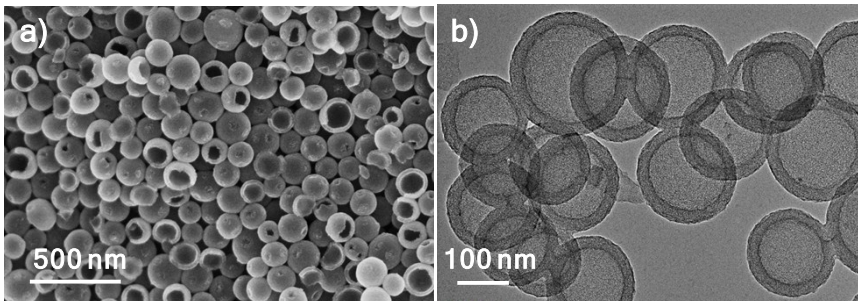

Fig. S3 a) SEM and b) TEM images of NHCS prepared by pyrolysis of NHCS-650 at 1000 ºC in Ar.

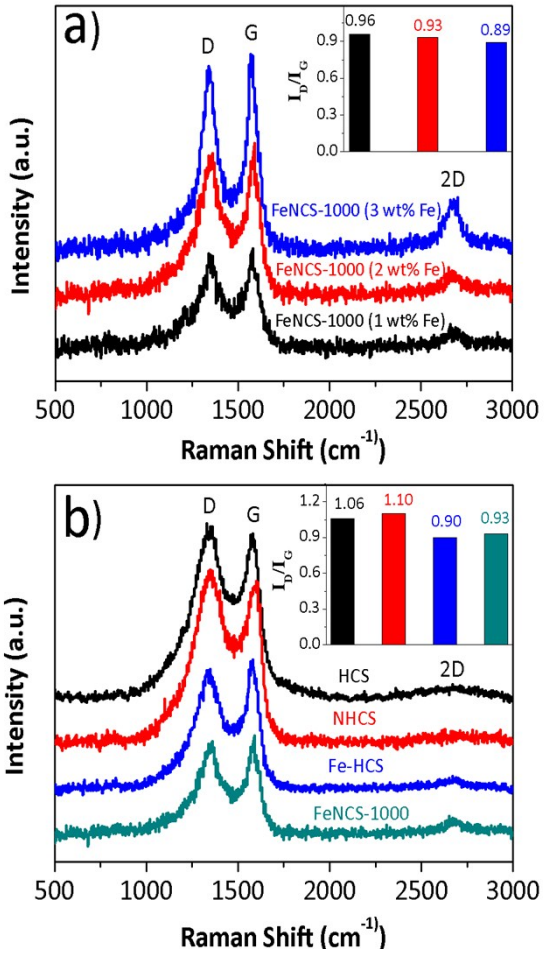

Fig. S4 a) Raman spectra of FeNCS-1000 prepared with 1, 2 and 3 wt% Fe, respectively. b) Raman spectra of HCS, NHCS, Fe-HCS and FeNCS-1000 (2 wt% Fe). The insets in a) and b) are the ratios of I_D to I_G for the corresponding samples. As illustrated in the histograms in Fig. S4, the value for I_D /I_G of FeNCS-1000 decreases with increasing Fe content, indicating that Fe source can promote

the graphitization of carbon material and higher pyrolysis temperature results in higher graphitization degree for Fe-doped samples.

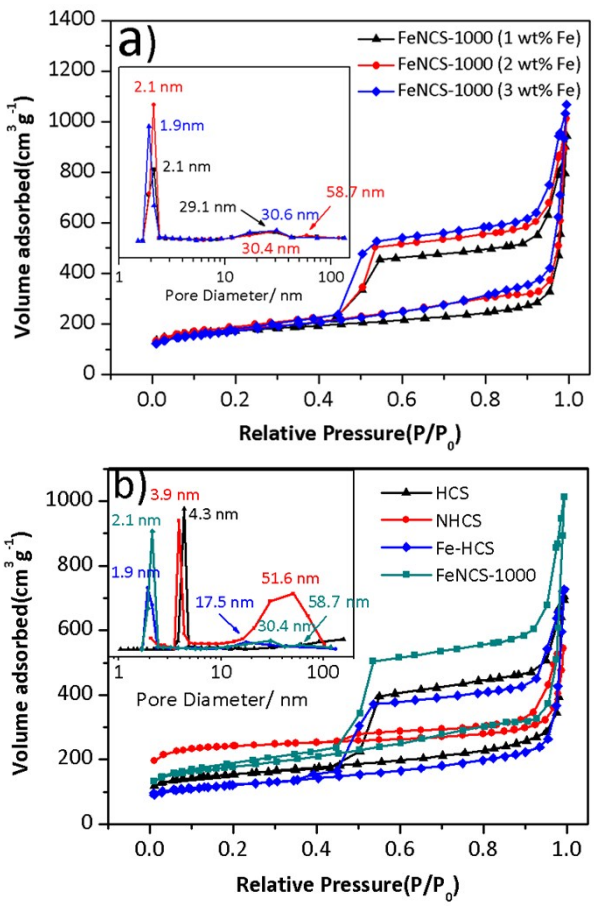

Fig. S5 Nitrogen adsorption-desorption isotherms and pore-size distributions (insets) of a) FeNCS-1000 with different Fe content and b) HCS, NHCS, Fe-HCS and FeNCS-1000. As shown in Fig. S5, except for the small mesopores at ~2 nm, another pores of 17.5-58.7 nm were also observed for FeNCS-1000. In addition, only one single pore (4.3 nm) could be observed for HCS, but N-doped HCS (NHCS) created new pore centered at 51.6 nm. The pores of FeNCS-1000 decreased to 2.1 and 30.4 nm compared with that of NHCS (3.9 and 51.6 nm), and new pore (58.7 nm) was formed. This is because of further shrinkage and enhanced graphitization of the carbon spheres due to the introduction of Fe source.

Table S1. Comparison for the texture parameters including BET surface area, pore size and pore volume of FeNCSs prepared with 2 wt% Fe at different temperature. The N_2 sorption isotherms are shown in Fig. 1 of the main text.

Samples	S_{BET}[a] (m^2 g^{-1})	V_{total}[b] (cm^3 g^{-1})	Pore size[c] (nm)
FeNCS-800	597	0.99	2.1, 17.5-58.7
FeNCS-900	524	1.10	2.1, 17.5-58.7
FeNCS-1000	613	1.57	2.1, 17.5-58.7
FeNCS-1100	423	1.04	1.9, 17.5-58.7

[a]Determined by the BET method at P/P_0 of 0.05–0.15. [b]Total pore volume for pores with Radius less than 1640.51 Å at P/Po = 0.99. [c]Maxima of the pore size distribution determined by the BJH method desorption data.

Table S2. Comparison for the texture parameters including BET surface area, pore size and pore volume of FeNCS-1000 with different Fe content.

Samples	S_{BET}[a] (m^2 g^{-1})	V_{total}[b] (cm^3 g^{-1})	Pore size[c] (nm)
FeNCS-1000 (*1 wt% Fe*)	593	1.46	2.1, 17.5-58.7
FeNCS-1000 (*2 wt% Fe*)	613	1.57	2.1, 17.5-58.7
FeNCS-1000	600	1.65	1.9, 17.5-58.7

(*3 wt% Fe*)

[a]Determined by the BET method at P/P_0 of 0.05–0.15. [b]Total pore volume for pores with Radius less than 1640.51 Å at P/Po = 0.99. [c]Maxima of the pore size distribution determined by the BJH method desorption data.

Table S3. Comparison for the texture parameters including BET surface area, pore size and pore volume of HPS, HCS, Fe-HCS, NHCS and FeNCS-1000 (2 wt% Fe).

Samples	S_{BET}[a] (m^2 g^{-1})	V_{total}[b] (cm^3 g^{-1})	Pore size[c] (nm)
HPS	455	0.35	3.8
HCS	524	0.48	4.3
Fe-HCS	419	1.13	1.9, 17.5
NHCS	820	0.56	3.9, 51.6
FeNCS-1000	613	1.57	2.1, 17.5-58.7

[a]Determined by the BET method at P/P0 of 0.05–0.15. [b]Total pore volume for pores with Radius less than 1640.51 Å at P/Po = 0.99. [c]Maxima of the pore size distribution determined by the BJH method desorption data.

Table S4. The contents of C, O, N and relative N species analyzed by N1s XPS spectra of the FeNCSs prepared at different temperature of 800-1100 ºC.

Samples	C[a] (at%)	O[a] (at%)	N[a] (at%)	pyridinic-N[b] (at%)	Fe-N_x[b] (at%)	graphitic-N[b] (at%)	oxidized-N[b] (at%)
FeNCS-800	85.4	6.4	7.6	39.92	27.13	23.26	9.69
FeNCS-900	87.4	7.1	5.0	36.77	28.81	25.27	9.15

FeNCS-1000	91.5	5.7	2.5	23.41	38.85	28.86	8.88
FeNCS-1100	93.5	4.7	1.6	15.60	29.25	47.76	7.68

[a]The C, O, N and Fe content of FeNCS-800, 900, 1000 and 1100. [b]The atomic percentage of the relative N species occupying in the total N content.

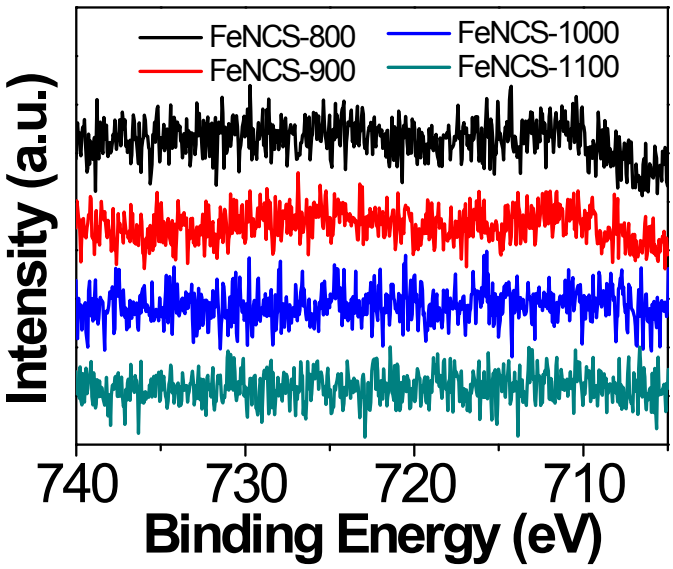

Fig. S6 High-resolution Fe 2p spectra for FeNCSs. No evident peaks could be found ascribed to low doping content of Fe.

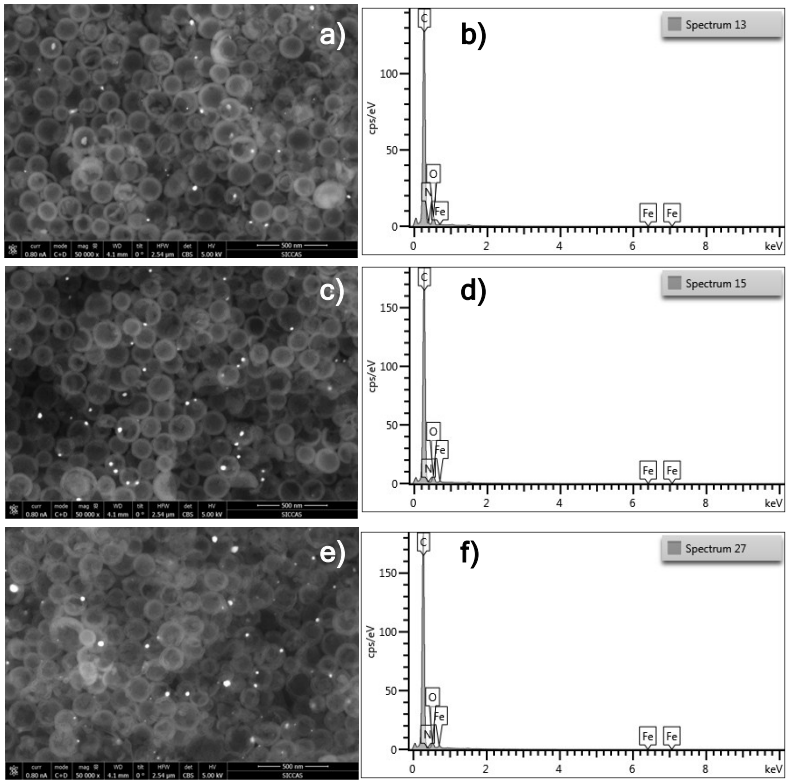

Fig. S7 STEM images and EDS spectra of FeNCSs prepared with different Fe/C mass ratios in the precursors at 1000 °C. a, b) Fe/C = 1 wt%; c, d) Fe/C = 2 wt%; and e, f) Fe/C = 3 wt%.

Table S5. The C, O, and Fe contents of FeNCSs prepared with different Fe/C mass ratios in the precursors at 1000 °C determined by EDS analysis.

Fe/C mass ratio in the precursor	C (wt%)	O (wt%)	Fe (wt%)
1 wt%	93.71	3.86	1.23
2 wt%	94.10	2.98	2.36
3 wt%	92.73	2.23	3.41

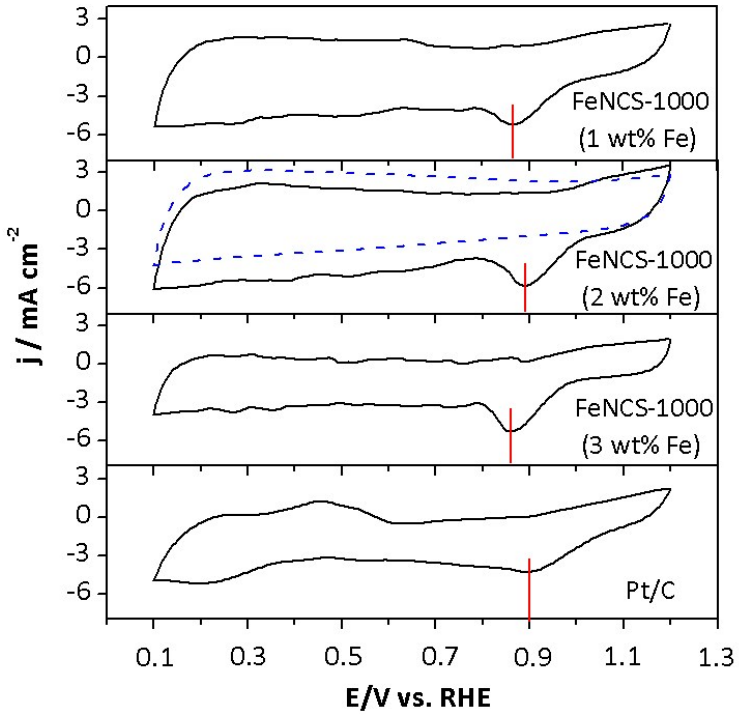

Fig. S8 Cycle voltammetry (CV) curves of (a) FeNCS-1000 with 1, 2 and 3 wt% Fe and commercial 20 wt% Pt/C catalyst in O_2-saturated 0.1 M KOH solution. Blue line in FeNCS-1000 is the CV curve obtained in N_2-saturated 0.1 M KOH solution. The cathodic ORR current peak positions for these samples follow the order: Pt/C (0.900 V) > FeNCS-1000 (2 wt% Fe, 0.891 V) > FeNCS-1000 (1 wt% Fe, 0.866 V) FeNCS-1000 (3 wt% Fe, 0.860 V).

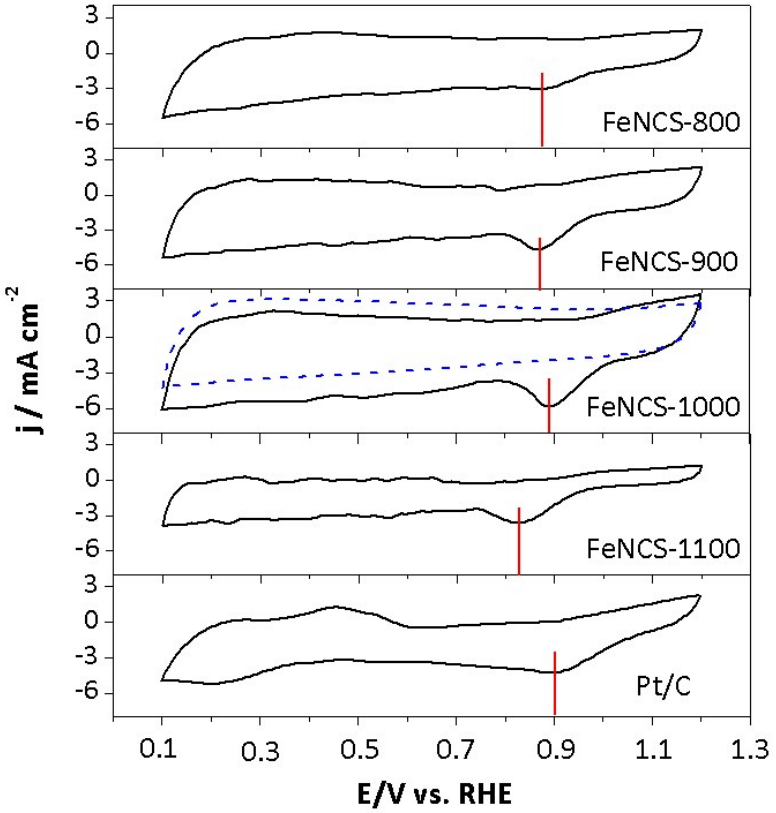

Fig. S9 Cycle voltammetry (CV) curves of FeNCSs prepared at different pyrolysis temperatures (800-1100 °C) and commercial 20 wt% Pt/C catalyst in O_2-saturated 0.1 M KOH solution. Blue line in FeNCS-1000 is the CV curve obtained in N_2-saturated 0.1 M KOH solution. The cathodic ORR current peak positions for these samples follow the order: Pt/C (0.900 V) > FeNCS-1000 (0.891 V) > FeNCS-800 (0.873) > FeNCS-900 (0.870 V) > FeNCS-1100 (0.828 V).

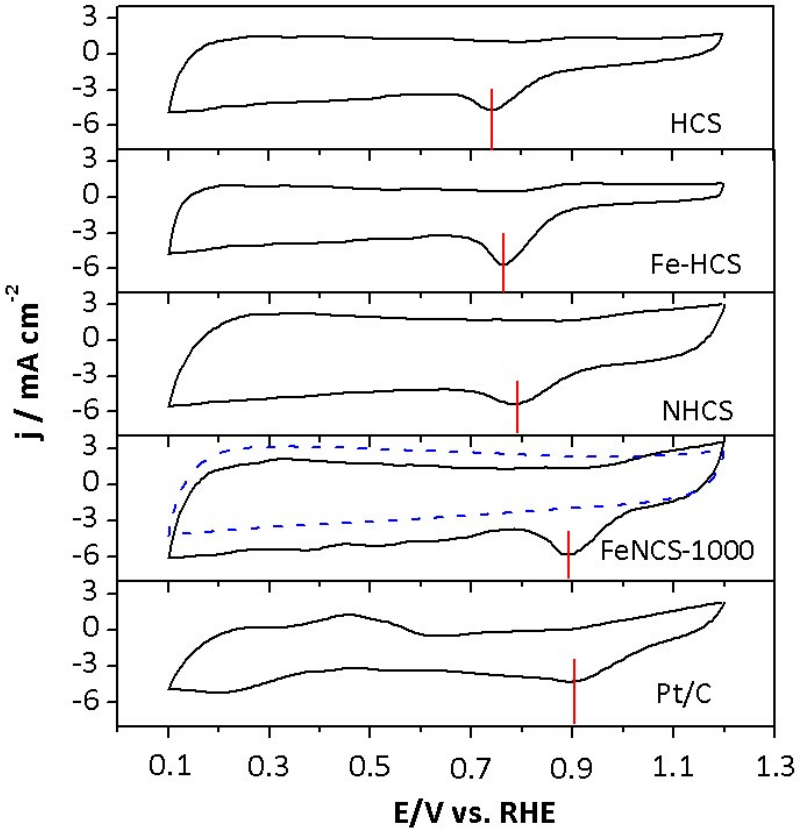

Fig. S10 Cycle voltammetry (CV) curves of HCS, Fe-HCS, NHCS, FeNCS-1000 and commercial Pt/C catalyst in O_2-saturated 0.1 M KOH solution. Blue line in FeNCS-1000 is the CV curve measured in N_2 saturated 0.1 M KOH solution. It is evident that the cathodic ORR peak position of FeNCS-1000 is very close to that of Pt/C, which is much more positive than those for HCS, Fe-HCS, and NHCS.

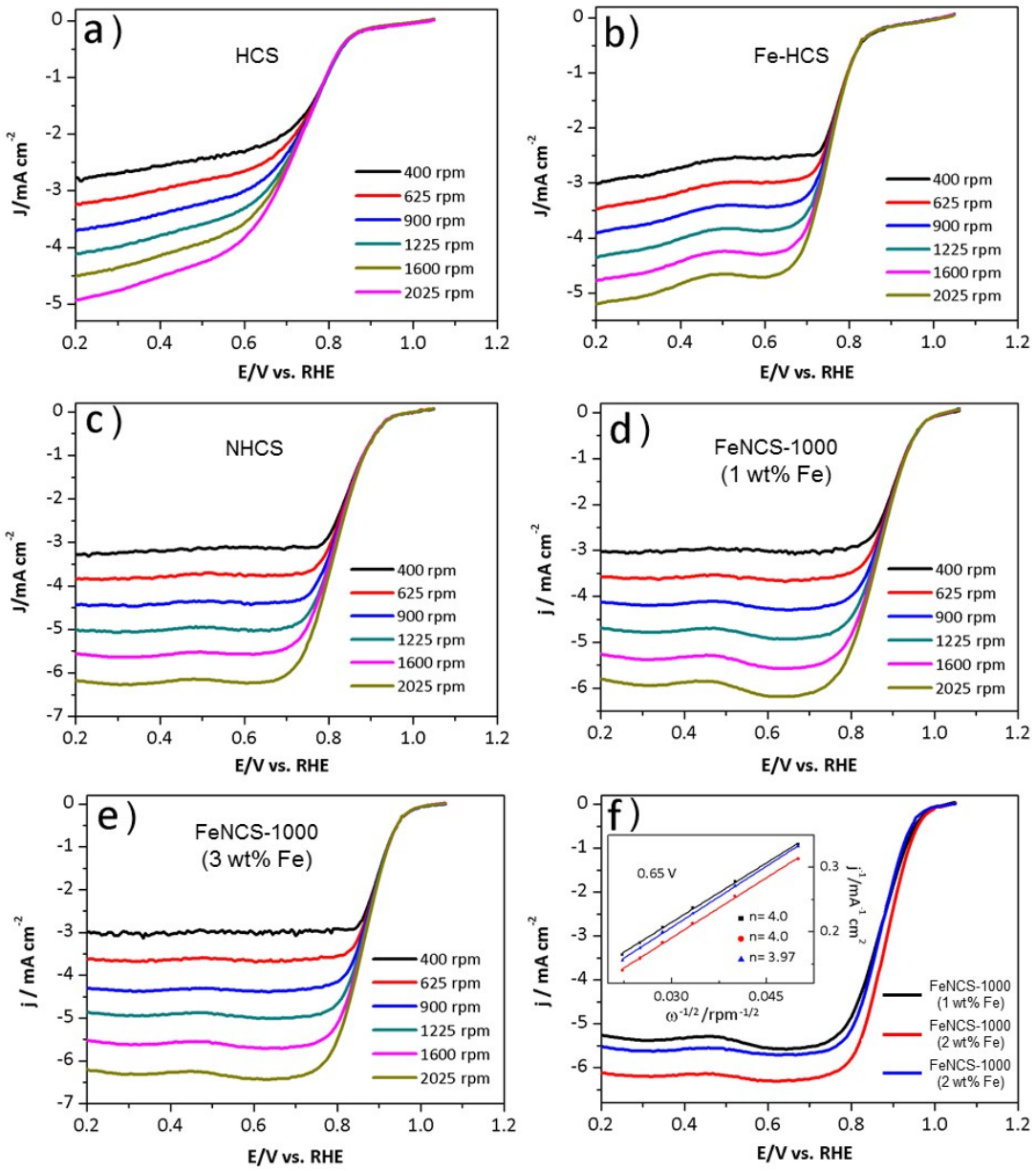

Fig. S11 RDE curves of a) HCS, b) Fe-HCS, c) NHCS, d) and e) FeNCS-1000 with 1 and 3 wt% Fe at various rotation speeds from 400 to 2025 rpm in O_2 saturated 0.1 M KOH solution (scanning rate: 10 mV s^{-1}), respectively. f) RDE curves of FeNCS-1000 with different Fe content at 1600 rpm in O_2 saturated 0.1 M KOH solution (scanning rate: 10 mV s^{-1}). The inset in f) is the corresponding Koutecky-Levich (K-L) plots of FeNCS-1000 with different Fe content at 0.65 V vs. RHE, respectively.

RDE curves of all samples for ORR at different rotating speeds from 400 to 2025 rpm indicate the increased current density with an increase in rotating speeds because of the improved mass transport on the electrode surface. As shown in Fig. S11f, the RDE curves obtained at 1600 rpm indicate that

FeNCS-1000 prepared with 2 wt% Fe shows the more positive $E_{1/2}$ value and larger limiting current density than FeNCS-1000 prepared with 1 and 3 wt% Fe, implying the optimum ORR performance for FeNCS-1000 (2 wt%) among these samples.

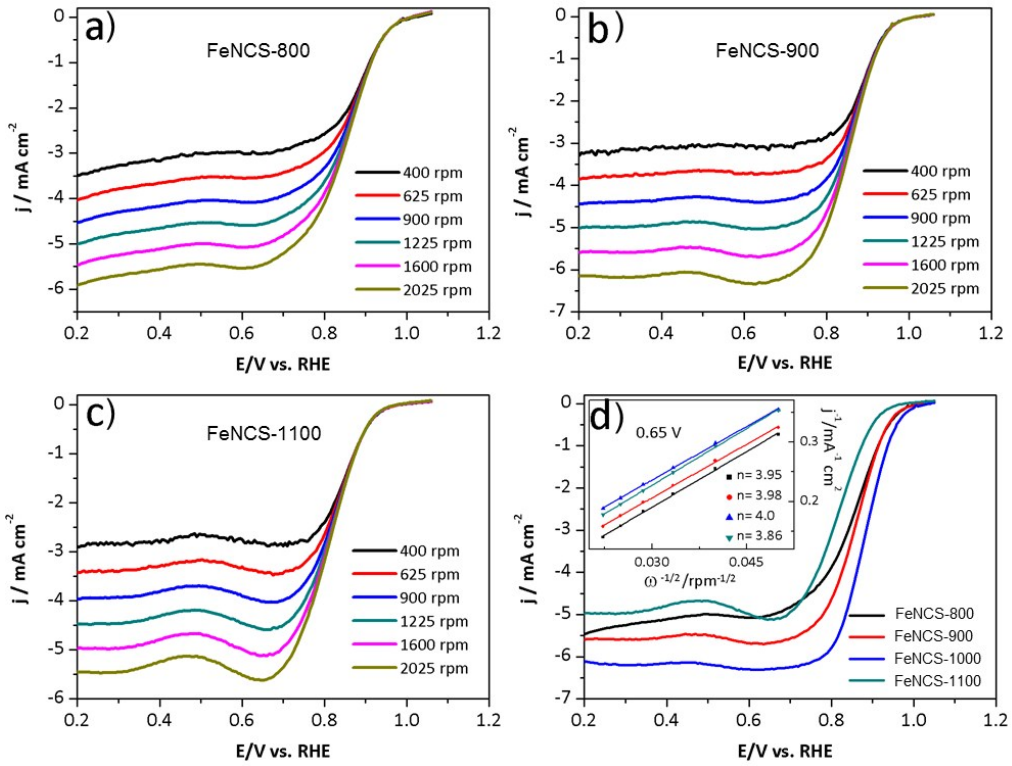

Fig. S12 RDE curves of a) FeNCS-800, b) FeNCS-900, c) FeNCS-1100 at various rotation speeds from 400 to 2025 rpm in O_2-saturated 0.1 M KOH solution (scanning rate: 10 mV s^{-1}), respectively. d) RDE curves of the FeNCS-800, FeNCS-900, FeNCS-1000 and FeNCS-1100 at 1600 rpm in O_2 saturated 0.1 M KOH solution (scanning rate: 10 mV s^{-1}). The inset in d) is the corresponding Koutecky-Levich (K-L) plots of the samples at 0.65 V vs. RHE.

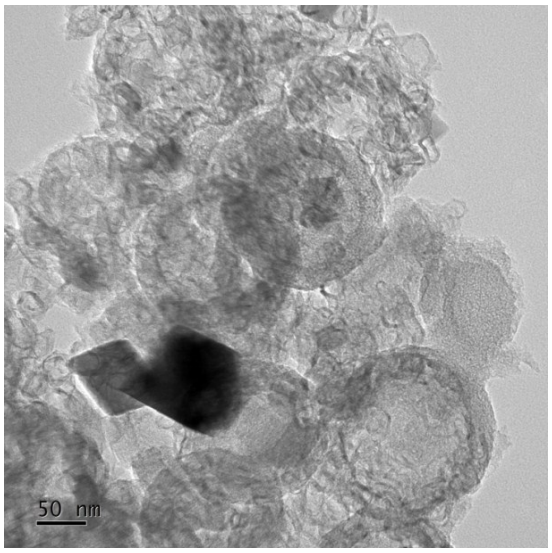

Fig. S13 TEM images of Fe-HCS. From the image, we can see that Fe-HCS demonstrates highly graphitized feature similar as FeNCS-1000. However, the activity of Fe-HCS is far lower than that of FeNCS-1000, suggesting that N-doping simultaneously plays a crucial role in FeNCS-1000 catalyst with outstanding performance for ORR. Besides, only N-doping can improve the activity for ORR, but it still can not match the high activity for FeNCS-1000 catalyst. Therefore，it can be concluded indirectly that the creation of Fe-N_x configurations should be main active sites of FeNCS-1000 for ORR.

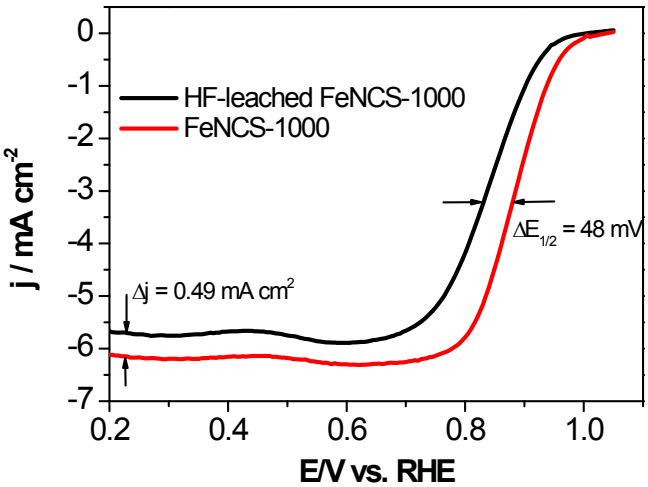

Fig. S14 Investigating the effects of HF treatment on FeNCS-1000 on the ORR activity in O_2-saturated 0.1 M KOH solution (rotating speed: 1600 rpm; scanning rate: 10 mV s^{-1}). It implies that HF treatment resulted in an evident decrease of the ORR activity in terms of $E_{1/2}$ and limiting current density.

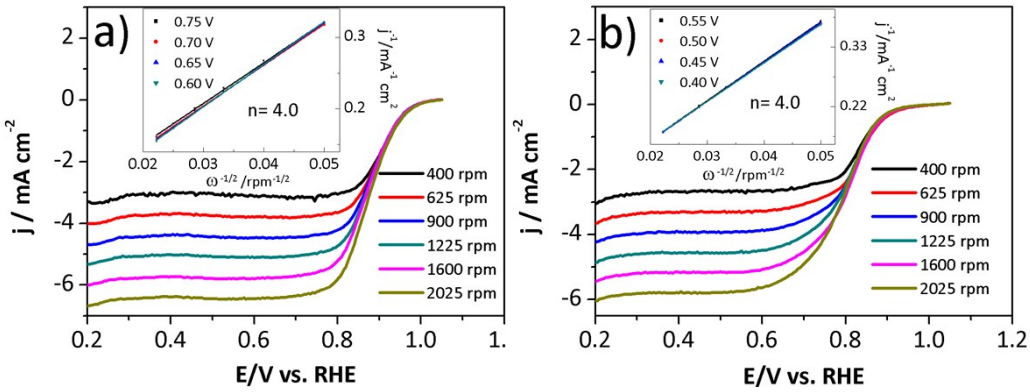

Fig. S15 RDE curves of 20 wt% Pt/C at various rotation speeds from 400 to 2025 rpm in O_2 saturated a) 0.1 M KOH solution and b) 0.5 M H_2SO_4 solution (scanning rate: 10 mV s^{-1}), respectively. The insets in a) and b) are the corresponding Koutecky-Levich (K-L) plots of Pt/C.

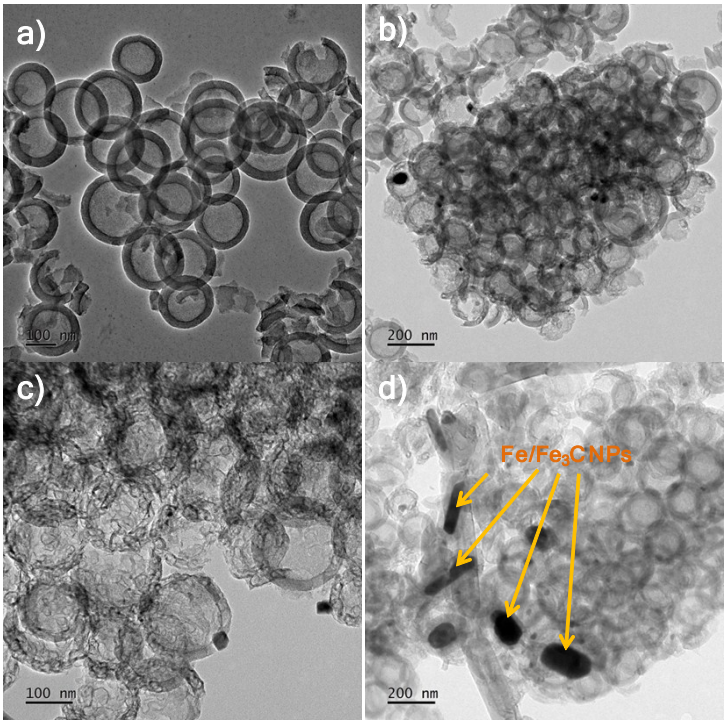

Fig. S16 TEM images of FeNCS-*X* prepared at different temperatures, a) 800, b) 900, c) 1000, and d) 1100 °C.

As shown in Fig. S16 a-d, all FeNCS-X samples show typical hollow particles. However, FeNCS-800 has amorphous carbon framework, consistent with the result of XRD analysis. It is evident that

the higher treatment temperature of 900-1100 ^{o}C results in the graphitization of mesoporous shells due to the existence of Fe elements within hollow spheres. Very large Fe/Fe_3C nanoparticles with sizes of nearly 200 nm are found in the 1100 ^{o}C-treated sample, due to the destruction of Fe-N_x moieties and the elimination of heteroatoms (e.g. Fe and N) at high temperature.

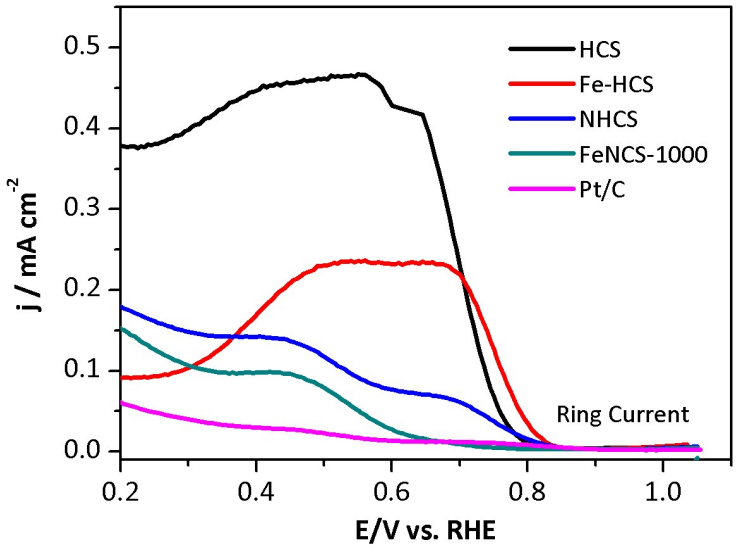

Fig. S17 Enlargement of the ring currents in Fig. 3d of the main text to highlight the difference.

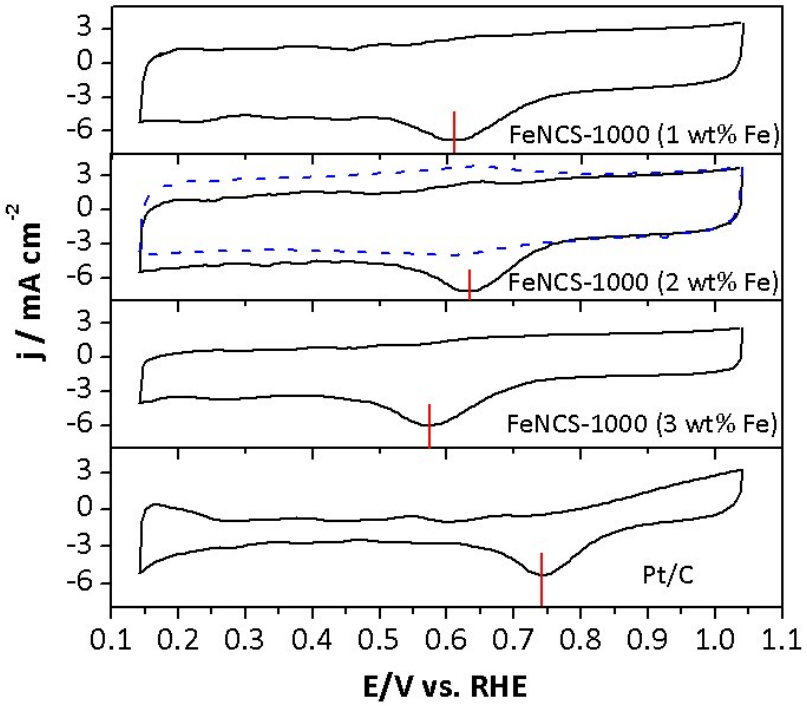

Fig. S18 Cycle voltammetry (CV) curves of FeNCS-1000 with 1, 2 and 3 wt% Fe and commercial Pt/C catalyst in O_2-saturated 0.5 M H_2SO_4 solution. Blue line for FeNCS-1000 is the CV curve measured in N_2-saturated 0.5 M H_2SO_4 solution. A well-defined oxygen reduction peak in CV curve is observed at 0.68 V in O_2-saturated 0.5 M H_2SO_4 solution, while there is no such a peak in N_2-saturated one (blue dashed line), suggesting that O_2 was reduced on the electrode coated with FeNCS-1000. The cathodic ORR current peak positions for these samples follow the order: Pt/C (0.738 V) > FeNCS-1000 (2 wt% Fe, 0.634 V) > FeNCS-1000 (1 wt% Fe, 0.609 V) FeNCS-1000 (3 wt% Fe, 0.572 V).

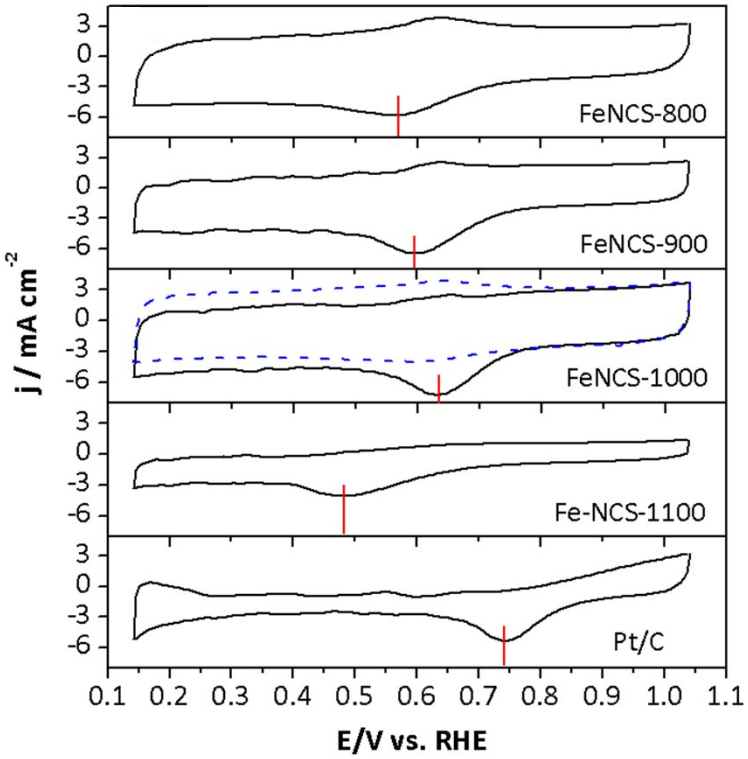

Fig. S19 Cycle voltammetry (CV) curves of FeNCS-800, 900, 1000, and 1100 and commercial Pt/C catalyst in O_2 saturated 0.5 M H_2SO_4 solution. Blue line for FeNCS-1000 is the CV curve measured in N_2 saturated 0.5 M H_2SO_4 solution. The cathodic ORR current peak positions for these samples follow the order: Pt/C (0.738 V) > FeNCS-1000 (0.634 V) > FeNCS-900 (0.597) > FeNCS-800 (0.567 V) > FeNCS-1100 (0.477 V).

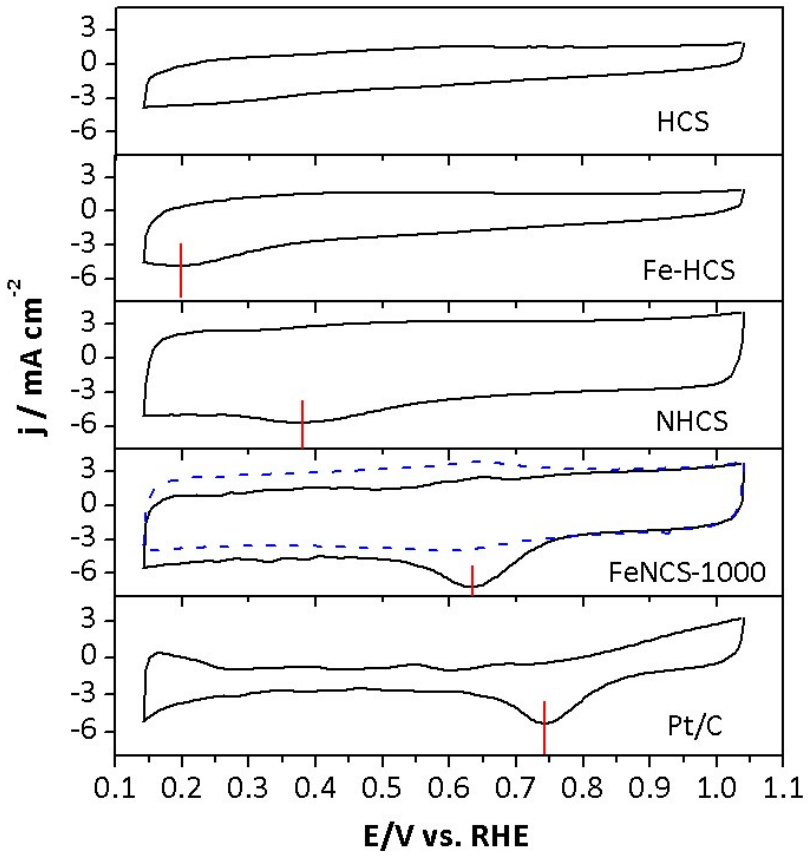

Fig. S20 Cycle voltammetry (CV) curves of HCS, Fe-HCS, NHCS, FeNCS-1000 and commercial Pt/C catalyst in O_2-saturated 0.5 M H_2SO_4 solution. Blue line for FeNCS-1000 is the CV curve measured in N_2 saturated 0.5 M H_2SO_4 solution.

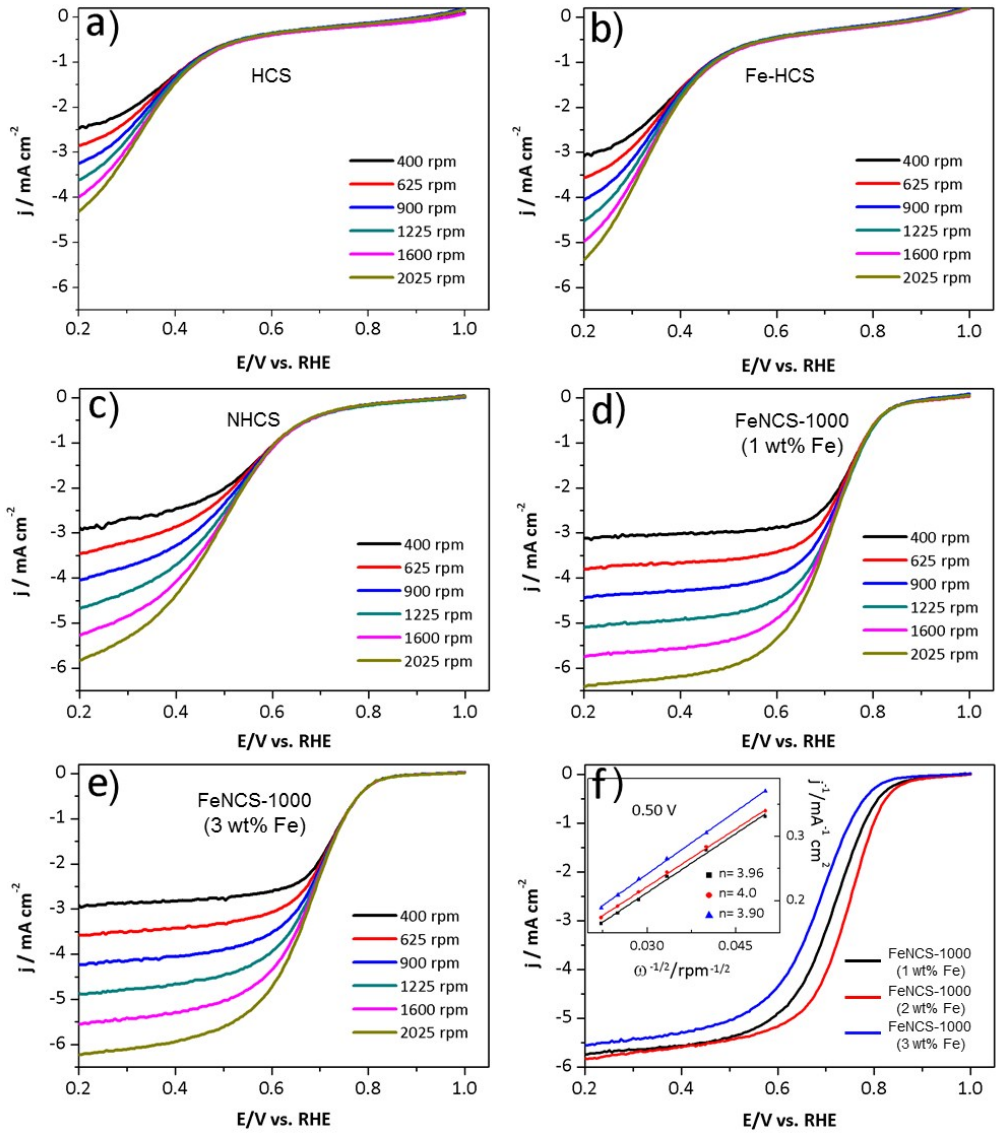

Fig. S21 RDE curves of the a) HCS, b) Fe-HCS, c) NHCS, d) and e) FeNCS-1000 with 1 and 3 wt% Fe at various rotation speeds from 400 to 2025 rpm in O_2 saturated 0.5 M H_2SO_4 solution (scanning rate: 10 mV s^{-1}), respectively. f) RDE curves of FeNCS-1000 with different Fe content at 1600 rpm in O_2 saturated 0.5 M H_2SO_4 solution (scanning rate: 10 mV s^{-1}). The inset in f) is the corresponding Koutecky-Levich (K-L) plots of the FeNCS-1000 with different Fe content at 0.50 V vs. RHE, respectively.

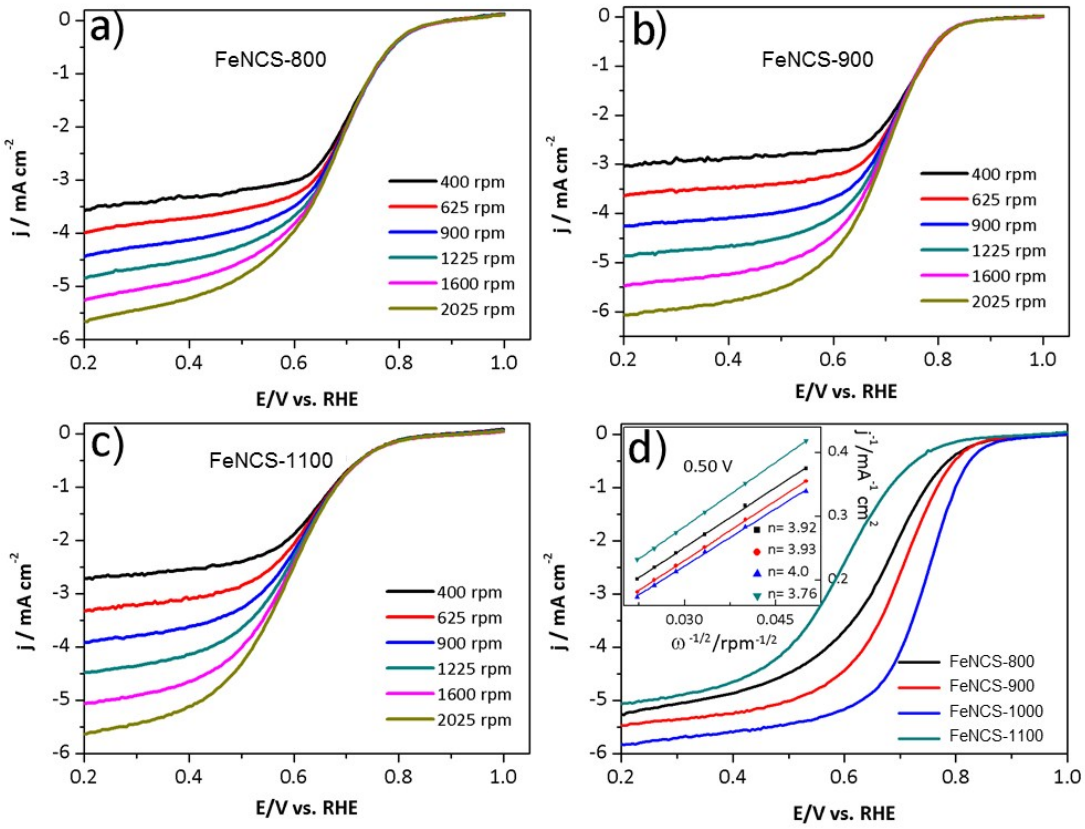

Fig. S22 RDE curves of a) FeNCS-800, b) FeNCS-900, c) FeNCS-1100 at various rotation speeds from 400 to 2025 rpm in O_2-saturated 0.5 M H_2SO_4 solution (scanning rate: 10 mV s^{-1}), respectively. d) RDE curves of the FeNCS-800, FeNCS-900, FeNCS-1000 and FeNCS-1100 at 1600 rpm in O_2-saturated 0.5 M H_2SO_4 solution (scanning rate: 10 mV s^{-1}). The inset in d) is the corresponding Koutecky-Levich (K-L) plots of the samples at 0.50 V vs. RHE.

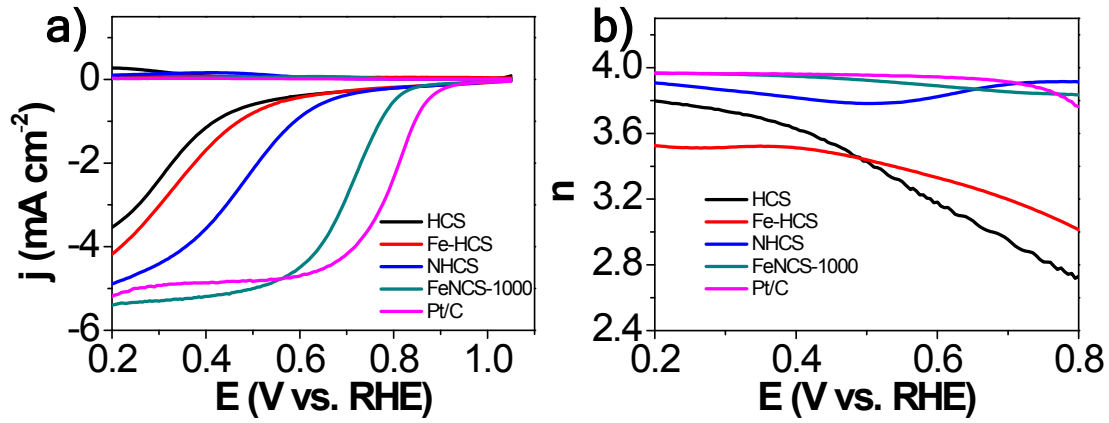

Fig. S23 RRDE voltammograms (rotating speed: 1600 rpm; scanning rate: 10 mV/s; ring potential: 1.2 V) and the calculated n values for HCS, Fe-HCS, NHCS, FeNCS-1000 and Pt/C.

Table S6. Comparison of the onset potential (E_{onset}), half-wave potential ($E_{1/2}$), current density at o.6 V (j @0.6 V), electron transfer number at 0.6 V (n @0.6 V) and H_2O_2 yield at 0.6 V (H_2O_2 yield @0.6 V) for ORR of non-noble metal catalysts systems from literature reprints and this work in alkaline medium (1600 rpm). The electron transfer number (n) was measured by the RRDE test.

Samples	Post-treatment	Loading (μg cm^{-2})	Electrolyte	E_{onset} (V. vs RHE)	$E_{1/2}$ (V. vs RHE)	J @0.6 V (mA cm^{-2})	n @0.6 V	H_2O_2 yield @0.6 V	Ref.
FeNCS-1000	-	495	0.1 M KOH	1.048	0.886	6.30	3.96	2.06	This work
Fe-N-CC	HF	100	0.1 M KOH	0.94	0.83	4.03	3.88	5.00	1
Fe-NMCSs	-	255	0.1 M KOH	1.027	0.86	5.34	3.99	0.84	2
Fe−N/C−700	Hot HCl	150	0.1 M KOH	0.956	0.840	6.03	3.96	1.76	3
FP-Fe-TA-N-850	HCl	300	0.1 M KOH	0.98	0.82	5.0	3.76	N.M	4
Fe−N−GC-900	HF	200	0.1 M KOH	1.01	0.86	5.0	[a]4.0	A.M	5
CoP-CMP800	-	600	0.1 M KOH	0.88	0.82	4.5	3.86	7.0	6
meso/micro-Fe-N-CNTs	Hot HF and HCl	400	0.1 M KOH	1.01	0.87	5.75	3.97	0.88	7
N-Fe-co-doped CNTs	HCl	485	0.1 M KOH	1.01	0.875	5.58	3.95	2.48	8
Fe–N-graphene	HCl	400	0.1 M KOH	1.01	0.801	9.0	3.98	1.23	9
Fe-N/C	-	800	0.1 M KOH	0.98	0.88	5.9	3.96	2.01	10
Fe_3C/NCNTs	-	1200	0.1 M KOH	1.013	0.861	5.73	3.94	3.21	11
Fe-N-CNFs	Hot H_2SO_4	600	0.1 M KOH	0.945	0.825	5.01	[a]3.93	N.M	12
S-Fe/NGC	Hot H_2SO_4	160	0.1 M KOH	0.91	0.84	4.5	3.98	0.98	13
FePhen@MOF-$ArNH_3$	-	600	0.1 M KOH	1.03	0.86	4.72	N.M	N.M	14

Fe−N/C-800	HCl	100	0.1 M KOH	0.923	0.809	5.84	3.99	0.68	15
Fe_3C@NCNF-900	-	150	0.1 M KOH	0.963	0.877	4.17	[a]3.8	N.M	16
CCOP-P-Fe	HCl	200	0.1 M KOH	0.98	0.77	3.9	3.82	9.16	17
Fe/Fe_2O_3@Fe-N-C-1000	Hot H_2SO_4	611	0.1 M KOH	0.925	0.795	6.25	[a]4.0	N.M	18
Fe-N/C-800	-	79.6	0.1 M KOH	0.98	0.82	4.68	3.96	2.02	19
Co_3O_4/N-rGO	-	100	0.1 M KOH	0.92	0.83	5.49	3.89	5.49	20
NC-foam	-	580	0.1 M KOH	0.95	0.80	4.0	3.62	19.0	21
Fe@C-FeNC-2	HNO_3	700	0.1 M KOH	1.016	0.899	5.08	3.96	1.30	22
Fe/Co-NpGr	Hot H_2SO_4	2500	0.1 M KOH	0.93	0.82	3.49	[a]4.0	N.M	23
$(Fe_2N/MNGCS)_4$	Hot HCl	400	0.1 M KOH	0.960	0.881	7.19	3.96	2.50	24
Fe-N-C	-	500	0.1 M KOH	0.991	0.837	6.68	3.82	8.72	25
Co-N-mC	-	283	0.1 M KOH	0.940	0.851	4.75	[a]3.7	N.M	26
Fe,S/NGC-900	Hot HCl	200	0.1 M KOH	0.95	0.83	5.18	3.99	1.22	27
3D Fe-N-C hybrid	-	600	0.1 M KOH	0.970	0.869	5.10	3.96	2.08	28
CNT/(N–C)-800	HF	100	0.1 M KOH	0.970	0.844	5.63	[a]4.0	N.M	29
Fe_3C@N-CNT assemblies	-	250	0.1 M KOH	0.97	0.85	5.62	[a]3.96	N.M	30
Co-NC	-	210	0.1 M KOH	0.95	0.83	4.4	[a]3.67	N.M	31
Fe_3O_4/N-GAs	-	-	0.1 M KOH	0.84	0.56	1.9	3.8	10.1	32
$MnCo_2O_4$/N-rGO	HCl	100	1 M KOH	0.95	0.86	3.75	3.9	5.0	33
HNCS71	HCl	500	0.1 M KOH	0.97	0.82	5.9	3.95	2.54	34
MB-CFs	HF	225	0.1 M KOH	0.99	0.81	4.8	[a]3.95	N.M	35

[a]Calculated based on the K-L equation.

Table S7. Comparison of the onset potential, half-wave potential, current density at o.6 V (j @0.6 V vs RHE), electron transfer number at 0.6 V (n @0.6 V vs RHE) and H_2O_2 yield at 0.6 V (H_2O_2 yield @0.6 V vs RHE) for ORR of non-noble metal catalysts systems from literature reprints and this work in acid medium (1600 rpm if not otherwise specified). The electron transfer number (n) was measured by the RRDE tests.

Samples	Post-treatment	Loading (μg cm^{-2})	Electrolyte	E_{onset} vs RHE	$E_{1/2}$ vs RHE	J @0.6 V	n @0.6 V Vs RHE	H_2O_2 yield @0.6 V	Ref.
FeNCS-1000	-	495	0.5 M H_2SO_4	0.910	0.750	5.17	3.89	5.54	This work
Fe-N-CC	HF	100	0.5 M H_2SO_4	0.80	0.52	1.30	3.83	8.12	1
Fe-NMCSs	-	255	0.1 M $HClO_4$	0.849	0.750	4.86	3.87	6.25	2
Fe−N/C−700	Hot HCl	150	0.1 M $HClO_4$	0.830	0.661	4.17	3.97	1.72	3
FP-Fe-TA-N-850	HF	300	0.1 M $HClO_4$	0.83	0.58	2.6	[a]3.2	N.M	4
Fe−N−GC-900	HF	600	0.1 M $HClO_4$	0.87	0.74	5.3	3.90	5.1	5
Co-N-C	-	600	0.5 M H_2SO_4	0.74	0.64	3.5	3.93	3.50	6
meso/micro-Fe-N-CNTs	Hot HF and HCl	400	0.1 M $HClO_4$	0.89	0.75	5.06	3.86	6.98	7
N-Fe-co-doped CNTs	HCl	485	0.1 M $HClO_4$	0.89	0.76	5.5	3.94	3.18	8
Fe–N-graphene	HCl	400	0.1 M	0.91	0.73	9.0	3.98	1.25	9

			$HClO_4$						
Fe-N-C	-	800	0.1 M $HClO_4$	0.92	0.79	5.2	3.85	7.50	10
Fe_3C/NCNTs	-	1200	0.5 M H_2SO_4	0.886	0.608	3.50	3.90	4.07	11
Fe-N-CNFs	Hot H_2SO_4	600	0.5 M H_2SO_4	0.748	0.563	1.75	[a]3.70	N.M	12
S-Fe/NGC	Hot H_2SO_4	160	0.1 M $HClO_4$	0.83	0.66	2.9	3.94	2.50	13
FePhen@MOF-ArNH_3	-	600	0.1 M $HClO_4$	0.93	0.77	5.09	3.99	0.28	14
Fe−N/C-800	HCl	100	0.1 M $HClO_4$	0.788	0.592	2.96	3.97	1.50	15
Fe_3C@NCNF-900	-	150	0.1 M $HClO_4$	0.832	0.642	2.84	N.M	N.M	16
CCOP-P-Fe	-	200	0.1 M $HClO_4$	0.89	0.58	1.75	3.6	20.0	17
Fe/Fe_2O_3@Fe-N-C	Hot H_2SO_4	611	0.1 M $HClO_4$	0.718	0.558	1.90	N.M	N.M	18
Fe-N-rGO	Hot H_2SO_4	400	0.5 M H_2SO_4	0.818	0.617	2.25	3.70	7.74	36
FeNP-C	Hot H_2SO_4	600	0.5 M H_2SO_4	0.87	0.72	4.3	N.M	N.M	37
Co-N-GA	Hot H_2SO_4	611	0.5 M H_2SO_4	0.87	0.73	5.13	3.76	12.09	38
Fe–N/CNN3	Hot HCl	500	0.5 M H_2SO_4	0.83	0.58	1.48	N.M	N.M	39
10% Fe−N−C (750 °C)	HCl	612	0.1 M $HClO_4$	0.87	0.75	3.90	3.92	4.0	40

Fe–N–C-700	-	385	0.5 M H_2SO_4	0.828	0.656	2.28	3.97	1.56	41
Co-Mo-N	-	97	0.5 M H_2SO_4	0.810	0.569	1.50	3.68	16.0	42
Fe-N-C/CNTs (*400 rpm*)	-	1200	0.1 M $HClO_4$	0.83	0.67	1.86	N.M	N.M	43
PpPD-Fe-C	Hot H_2SO_4	900	0.5 M H_2SO_4	0.826	0.718	2.90	[a]3.8	N.M	44
Fe_3O_4/N-GAs	-	-	0.5 M H_2SO_4	0.75	0.34	N.M	3.95	2.4	32
Fe–AAPyr	HF	600	0.5 M H_2SO_4	0.90	0.75	5.17	3.94	3.03	45
Fe_3C/C-700 (*900 rpm*)	-	600	0.5 M H_2SO_4	0.90	0.73	3.58	3.87	6.63	46

[a]Calculated based on the K-L equation.

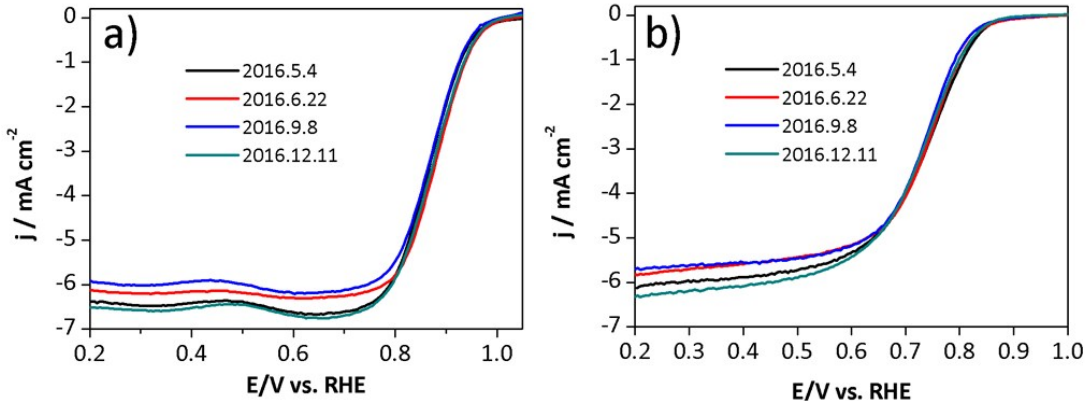

Fig. 24 LSV curves of four FeNCS-1000 samples synthesized at different dates from 2016.5.5 to 2016.12.11 in O_2-saturated a) 0.1 M KOH solution, b) 0.5 M H_2SO_4 solution (rotating speed: 1600 rpm; scanning rate: 10 mV s^{-1}), respectively. The FeNCS-1000 synthesized at 2016.6.22 (red lines) was used and compared in this article.

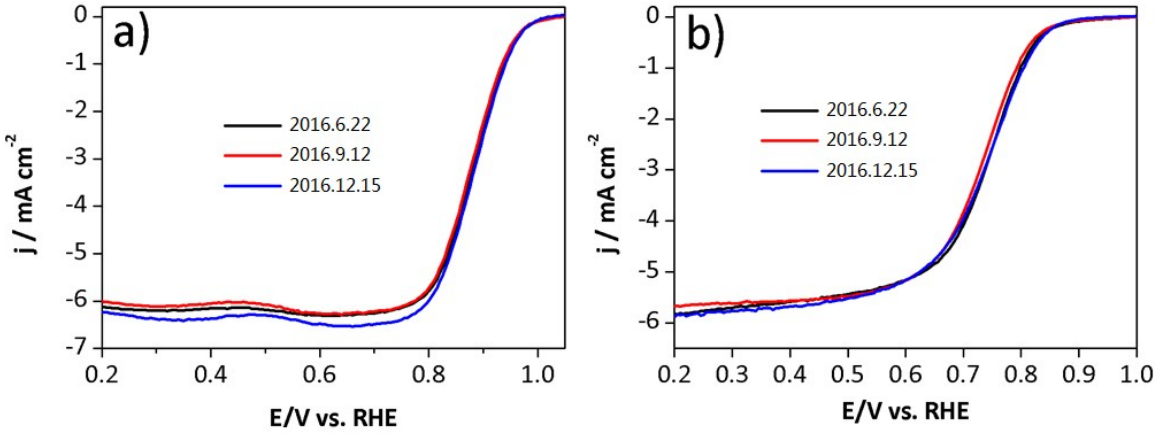

Fig. 25 LSV tests for FeNCS-1000 (synthesized at 2016.6.22) performed at different dates (2014.6.22, 2016.9.12, and 2016.12.15) in O_2-saturated a) 0.1 M KOH solution, b) 0.5 M H_2SO_4 solution (rotating speed: 1600 rpm; scanning rate: 10 mV s^{-1}), respectively. The LSV curves tested at 2016.6.22 (black lines) were used and compared in this article.

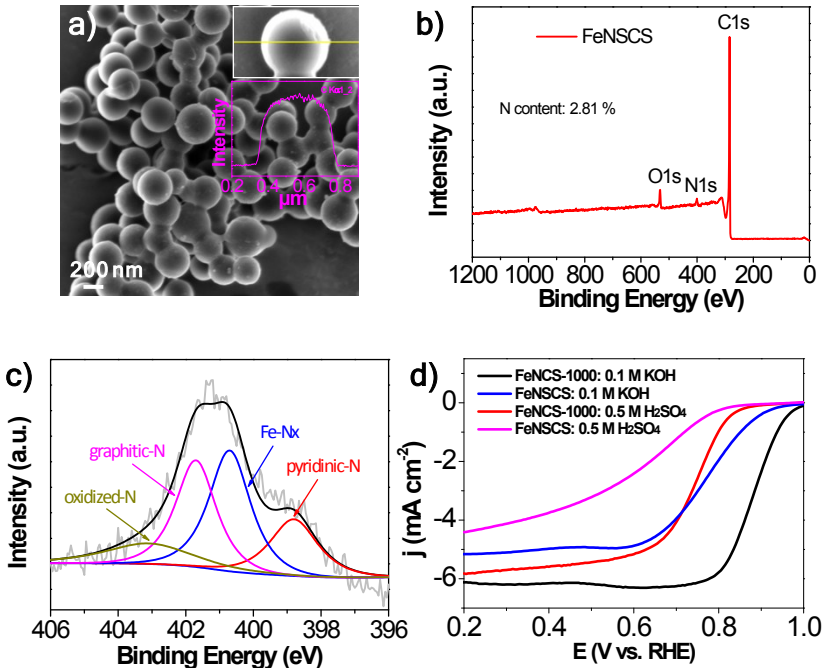

Fig. 26 a) SEM image (inset: a single FeNSCS sphere with a solid core proved by corresponding cross-sectional line scan for carbon element), b) XPS survey for FeNSCS, c) high-resolution N 1s XPS spectrum for FeNSCS, and d) comparison of RDE voltammograms for FeNSCS and FeNCS-1000 collected in 0.1 M KOH and 0.5 M H_2SO_4 (rotating speed: 1600 rpm; scanning rate: 10 mV s^{-1}), respectively.

Table S8. Comparison for N and Fe-N_x content of FeNSCS and FeNCS-1000.

Samples	N content (%)	pyridinic-N	graphitic-N	Fe-N_x	Oxidized-N
FeNSCS	2.8	19.56	31.23	36.37	12.54
FeNCS-1000	2.5	23.41	28.86	38.85	8.88

Table S9. Comparison for ORR activity in terms of the onset potential (E_{onset}), half-wave potential ($E_{1/2}$), current density at 0.6 V (j @0.6 V) of FeNCS@ and FeNCS-1000.

Samples	E_{onset} (V vs RHE)		$E_{1/2}$ (V vs RHE)		J @0.6 V vs RHE (mA cm^{-2})	
	0.1 M KOH	0.5 M H_2SO_4	0.1 M KOH	0.5 M H_2SO_4	0.1 M KOH	0.5 M H_2SO_4
FeNSCS	0.972	0.870	0.770	0.617	4.87	2.41
FeNCS-1000	1.048	0.910	0.886	0.760	6.30	5.17

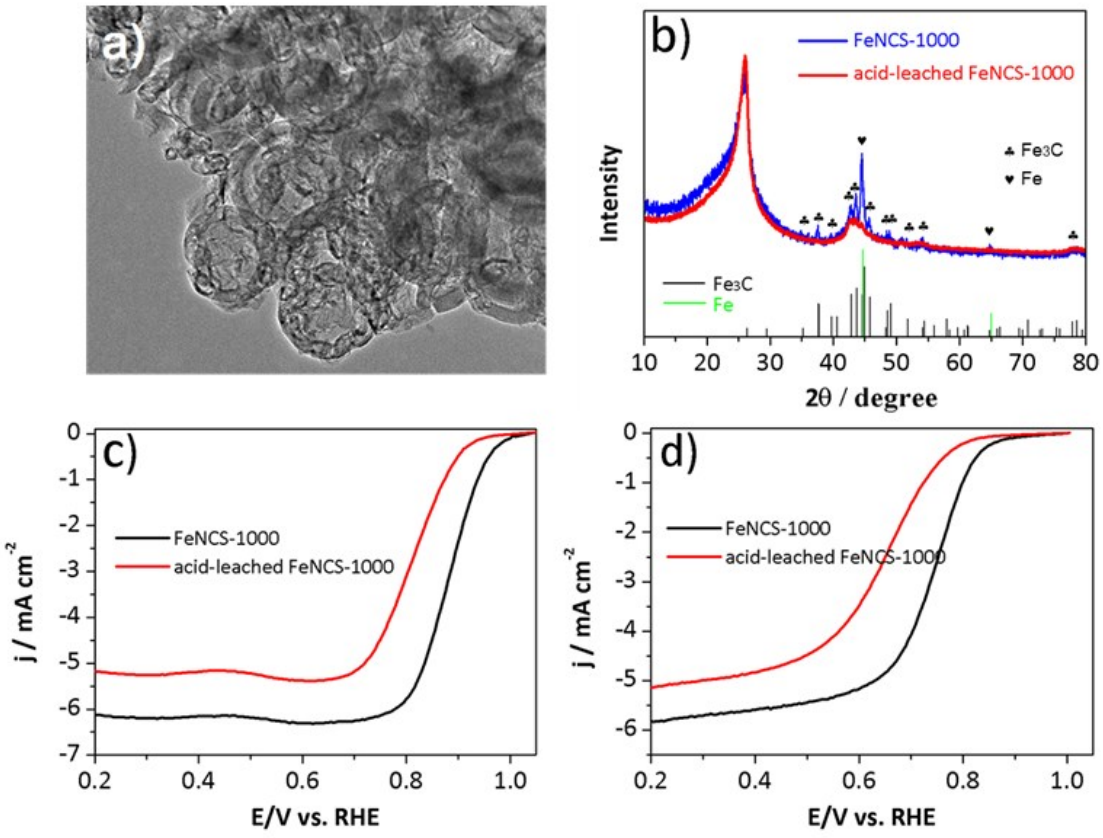

Fig. S27 a) TEM image of FeNCS-1000 after acid-leached treatment with 0.5 M hot H_2SO_4 solution (acid-leached FeNCS-1000), b) XRD patterns of FeNCS-1000 and acid-leached FeNCS-1000, c) and d) LSV curves of FeNCS-1000 and acid-leached FeNCS-1000 at 1600 rpm in O_2 saturated 0.1 M KOH and 0.5 M H_2SO_4 solution (scanning rate: 10 mV s^{-1}), respectively.

To demonstrate the effect of the Fe/Fe_3C nanocrystals on the ORR activity, the FeNCS-1000 was leached in 0.5 M H_2SO_4 at 60 °C for 12 h to remove the Fe/Fe_3C nanocrystals, which was denoted as acid-leached FeNCS-1000. TEM image and the XRD patterns indicate the removal of Fe_3C/Fe nanoparticles in FeNCS-1000 by acid-leaching treatment. It shows that acid-leached FeNCS-1000 has inferior ORR activity to original FeNCS-1000.

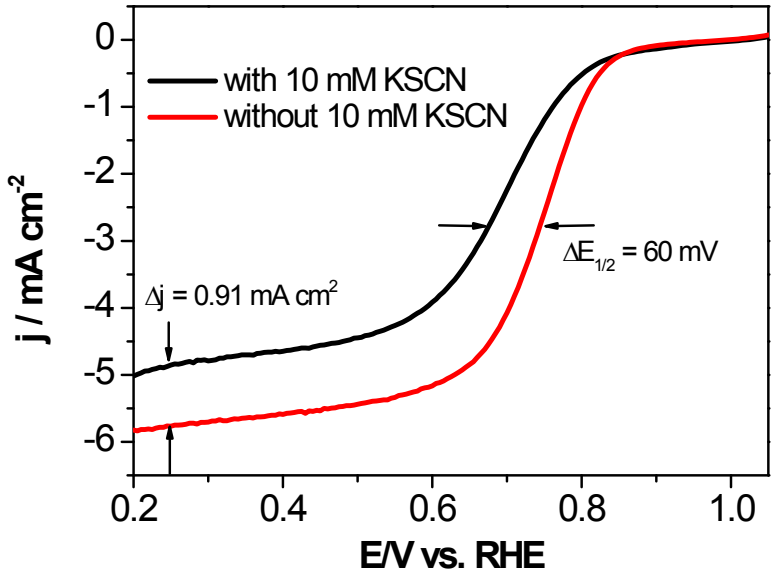

Fig. S28 RDE curves of FeNCS-1000 measured in O_2-saturated 0.5 M H_2SO_4 solution with or without 10 mM KSCN.

References for Electronic Supplementary Information:

1. G. A. Ferrero, K. Preuss, A. Marinovic, A. B. Jorge, N. Mansor, D. J. L. Brett, A. B. Fuertes, M. Sevilla and M.-M. Titirici, *ACS Nano*, 2016, **10**, 5922-5932.
2. F. L. Meng, Z. L. Wang, H. X. Zhong, J. Wang, J. M. Yan and X. B. Zhang, *Advanced materials*, 2016, **28**, 7948-7955.
3. Z. K. Yang, L. Lin and A. W. Xu, *Small*, 2016, **12**, 5710-5719.
4. J. Wei, Y. Liang, Y. Hu, B. Kong, G. P. Simon, J. Zhang, S. P. Jiang and H. Wang, *Angewandte Chemie*, 2016, **55**, 1355-1359.
5. A. Kong, X. Zhu, Z. Han, Y. Yu, Y. Zhang, B. Dong and Y. Shan, *ACS Catalysis*, 2014, **4**, 1793-1800.
6. Z.-S. Wu, L. Chen, J. Liu, K. Parvez, H. Liang, J. Shu, H. Sachdev, R. Graf, X. Feng and K. Müllen, *Advanced materials*, 2014, **26**, 1450-1455.
7. J.-C. Li, P.-X. Hou, C. Shi, S.-Y. Zhao, D.-M. Tang, M. Cheng, C. Liu and H.-M. Cheng, *Carbon*, 2016, **109**, 632-639.
8. Y. Li, W. Zhou, H. Wang, L. Xie, Y. Liang, F. Wei, J. C. Idrobo, S. J. Pennycook and H. Dai, *Nature nanotechnology*, 2012, **7**, 394-400.
9. C. He, J. J. Zhang and P. K. Shen, *Journal of Materials Chemistry A*, 2014, **2**, 3231.
10. Y. J. Sa, D. J. Seo, J. Woo, J. T. Lim, J. Y. Cheon, S. Y. Yang, J. M. Lee, D. Kang, T. J. Shin, H. S. Shin, H. Y. Jeong, C. S. Kim, M. G. Kim, T. Y. Kim and S. H. Joo, *Journal of the American Chemical Society*, 2016, DOI: 10.1021/jacs.6b09470.
11. W. Yang, X. Liu, X. Yue, J. Jia and S. Guo, *Journal of the American Chemical Society*, 2015, **137**, 1436-1439.
12. Z.-Y. Wu, X.-X. Xu, B.-C. Hu, H.-W. Liang, Y. Lin, L.-F. Chen and S.-H. Yu, *Angewandte Chemie International Edition*, 2015, **54**, 8179-8183.
13. K. Hu, L. Tao, D. Liu, J. Huo and S. Wang, *ACS applied materials & interfaces*, 2016, **8**, 19379-19385.
14. K. Strickland, E. Miner, Q. Jia, U. Tylus, N. Ramaswamy, W. Liang, M. T. Sougrati, F. Jaouen and S. Mukerjee, *Nat Commun*, 2015, **6**, 7343.
15. L. Lin, Q. Zhu and A. W. Xu, *Journal of the American Chemical Society*, 2014, **136**, 11027-11033.

16. G. Ren, X. Lu, Y. Li, Y. Zhu, L. Dai and L. Jiang, *ACS applied materials & interfaces*, 2016, **8**, 4118-4125.

17. Z. Xiang, Y. Xue, D. Cao, L. Huang, J.-F. Chen and L. Dai, *Angewandte Chemie International Edition*, 2014, **53**, 2433-2437.

18. Y. Zang, H. Zhang, X. Zhang, R. Liu, S. Liu, G. Wang, Y. Zhang and H. Zhao, *Nano Research*, 2016, **9**, 2123-2137.

19. W. Niu, L. Li, X. Liu, N. Wang, J. Liu, W. Zhou, Z. Tang and S. Chen, *Journal of the American Chemical Society*, 2015, **137**, 5555-5562.

20. Y. Liang, Y. Li, H. Wang, J. Zhou, J. Wang, T. Regier and H. Dai, *Nature materials*, 2011, **10**, 780-786.

21. J. Liu, B. V. Cunning, T. Daio, A. Mufundirwa, K. Sasaki and S. M. Lyth, *Electrochimica Acta*, 2016, **220**, 554-561.

22. W. J. Jiang, L. Gu, L. Li, Y. Zhang, X. Zhang, L. J. Zhang, J. Q. Wang, J. S. Hu, Z. Wei and L. J. Wan, *Journal of the American Chemical Society*, 2016, **138**, 3570-3578.

23. T. Palaniselvam, V. Kashyap, S. N. Bhange, J.-B. Baek and S. Kurungot, *Advanced Functional Materials*, 2016, **26**, 2150-2162.

24. J. Xiao, Y. Xu, Y. Xia, J. Xi and S. Wang, *Nano Energy*, 2016, **24**, 121-129.

25. X. Cui, S. Yang, X. Yan, J. Leng, S. Shuang, P. M. Ajayan and Z. Zhang, *Advanced Functional Materials*, 2016, **26**, 5708-5717.

26. F. Hu, H. Yang, C. Wang, Y. Zhang, H. Lu and Q. Wang, *Small*, 2016, DOI: 10.1002/smll.201602507.

27. B. Men, Y. Sun, J. Liu, Y. Tang, Y. Chen, P. Wan and J. Pan, *ACS applied materials & interfaces*, 2016, **8**, 19533-19541.

28. Y. Zhang, L.-B. Huang, W.-J. Jiang, X. Zhang, Y.-Y. Chen, Z. Wei, L.-J. Wan and J.-S. Hu, *J. Mater. Chem. A*, 2016, **4**, 7781-7787.

29. J. C. Li, S. Y. Zhao, P. X. Hou, R. P. Fang, C. Liu, J. Liang, J. Luan, X. Y. Shan and H. M. Cheng, *Nanoscale*, 2015, **7**, 19201-19206.

30. B. Y. Guan, L. Yu and X. W. Lou, *Energy Environ. Sci.*, 2016, **9**, 3092-3096.

31. A. Aijaz, J. Masa, C. Rosler, W. Xia, P. Weide, A. J. Botz, R. A. Fischer, W. Schuhmann and M. Muhler, *Angewandte Chemie*, 2016, **55**, 4087-4091.

32. Z. S. Wu, S. Yang, Y. Sun, K. Parvez, X. Feng and K. Mullen, *Journal of the American Chemical Society*, 2012, **134**, 9082-9085.

33. Y. Liang, H. Wang, J. Zhou, Y. Li, J. Wang, T. Regier and H. Dai, *Journal of the American Chemical Society*, 2012, **134**, 3517-3523.

34. J. Sanetuntikul, T. Hang and S. Shanmugam, *Chem. Commun*, 2014, **50**, 9473-9476.

35. C. Liu, J. Wang, J. Li, R. Luo, X. Sun, J. Shen, W. Han and L. Wang, *Carbon*, 2017, **114**, 706-716.

36. H. R. Byon, J. Suntivich and Y. Shao-Horn, *Chemistry of Materials*, 2011, **23**, 3421-3428.

37. Y. Hu, J. Zhu, Q. Lv, C. Liu, Q. Li and W. Xing, *Electrochimica Acta*, 2015, **155**, 335-340.

38. X. Fu, J. Y. Choi, P. Zamani, G. Jiang, M. A. Hoque, F. M. Hassan and Z. Chen, *ACS applied materials & interfaces*, 2016, **8**, 6488-6495.

39. E. Negro, A. H. A. M. Videla, V. Baglio, A. S. Aricò, S. Specchia and G. J. M. Koper, *Applied Catalysis B: Environmental*, 2015, **166-167**, 75-83.

40. M.-Q. Wang, W.-H. Yang, H.-H. Wang, C. Chen, Z.-Y. Zhou and S.-G. Sun, *ACS Catalysis*, 2014, **4**, 3928-3936.

41. H. Xiao, Z.-G. Shao, G. Zhang, Y. Gao, W. Lu and B. Yi, *Carbon*, 2013, **57**, 443-451.

42. T. Sun, Q. Wu, R. Che, Y. Bu, Y. Jiang, Y. Li, L. Yang, X. Wang and Z. Hu, *ACS Catalysis*, 2015, **5**, 1857-1862.

43. B. Merzougui, A. Hachimi, A. Akinpelu, S. Bukola and M. Shao, *Electrochimica Acta*, 2013, **107**, 126-132.

44. Y. Zhu, B. Zhang, X. Liu, D. W. Wang and D. S. Su, *Angewandte Chemie*, 2014, **53**, 10673-10677.

45. M. H. Robson, A. Serov, K. Artyushkova and P. Atanassov, *Electrochimica Acta*, 2013, **90**, 656-665.

46. Y. Hu, J. O. Jensen, W. Zhang, L. N. Cleemann, W. Xing, N. J. Bjerrum and Q. Li, *Angewandte Chemie*, 2014, **53**, 3675-3679.